

# Antiferromagnetic Order in the Rare Earth Halide Perovskites CsEuBr<sub>3</sub> and CsEuCl<sub>3</sub>

Daniel B. Straus,<sup>1\*</sup> Tomasz Klimczuk<sup>2,3</sup>, Xianghan Xu,<sup>1</sup> and Robert J. Cava<sup>1\*</sup>

<sup>1</sup>Department of Chemistry, Princeton University, Princeton, NJ 08544 USA

<sup>2</sup>Faculty of Applied Physics and Mathematics, Gdansk University of Technology,  
Narutowicza 11/12, 80-952, Gdansk, Poland

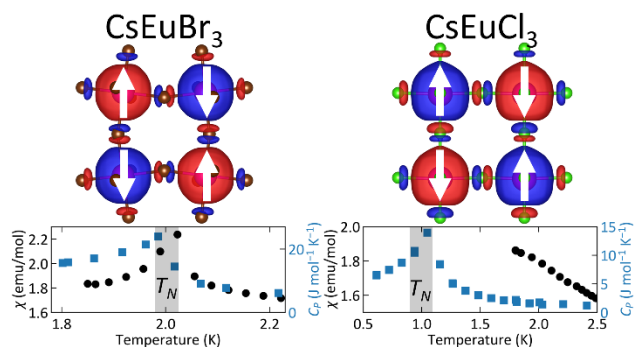
<sup>3</sup>Advanced Materials Centre, Gdansk University of Technology,  
Narutowicza 11/12, 80-952, Gdansk, Poland

\*Authors to whom correspondence should be addressed. Email: dstraus@princeton.edu,  
rcava@princeton.edu

## Abstract

Bulk CsEuBr<sub>3</sub> and CsEuCl<sub>3</sub> are shown to be magnetic semiconductors that order antiferromagnetically at Neel temperatures of 2.0 K and 1.0 K respectively. Given that nanoparticles and thin films of CsEuCl<sub>3</sub> have been reported to order ferromagnetically at a similar temperature, our observations of antiferromagnetic ordering in CsEuBr<sub>3</sub> and CsEuCl<sub>3</sub> expand the possible applications of halide perovskites to now include spintronic devices where both ferromagnetic and antiferromagnetic devices can be fabricated from a single material.

## TOC Graphic



Halide perovskites with the classical perovskite crystal structure are composed of a network of corner-sharing metal-halide octahedra, with the interstitial space occupied by a cation.<sup>1,2</sup> The choice of metal and cation is limited by size—if the cations are too large or too small, a halide perovskite cannot form.<sup>3,4</sup> Charge neutrality must also be obeyed—the metal is almost always in the 2+ oxidation state and the cation singly charged. Most of the metals that can form a halide perovskite are closed-shell, and magnetic ordering cannot occur because there are no unpaired spins.<sup>5</sup> The most studied halide perovskites contain the closed-shell metals  $\text{Pb}^{2+}$  or  $\text{Sn}^{2+}$  because these materials have very long carrier diffusion lengths and high absorption cross-sections,<sup>6</sup> allowing them to be used in high-performance solar cells with efficiencies rivaling commercial silicon-based solar cells.<sup>7,8</sup>

The spotlight on quantum materials has brought a renewed focus on developing new magnetic compounds that can be harnessed for spintronic applications, such as classical computers that have storage and logic in a single computational unit as well as quantum computers.<sup>9–15</sup> The magnetic  $\text{KMF}_3$  ( $\text{M} = \text{Mn}^{2+}$ ,  $\text{Fe}^{2+}$ ,  $\text{Co}^{2+}$ ,  $\text{Ni}^{2+}$ , or  $\text{Cu}^{2+}$ ) perovskites were synthesized in the 1960s and all order antiferromagnetically.<sup>16,17</sup>  $\text{KMnCl}_3$  is another antiferromagnetic halide perovskite,<sup>18</sup> but it is not stable and spontaneously converts into a non-perovskite phase like the halide perovskite  $\text{CsPbI}_3$ .<sup>19,20</sup> There are very few magnetic chloride, bromide, and iodide halide perovskites because open-shell 2+ transition metals are too small to form a stable perovskite, though some can be incorporated into magnetic layered two-dimensional organic-inorganic hybrid halide perovskites because the reduced dimensionality relaxes some structural constraints.<sup>5,21</sup>

Rare earth ions provide another way to form three-dimensional magnetic halide perovskites. Specifically,  $\text{Eu}^{2+}$  has an unpaired electron in each of its seven 4*f* orbitals, allowing for magnetic interactions between  $\text{Eu}^{2+}$  ions. The perovskites  $\text{CsEuX}_3$  ( $\text{X} = \text{Cl}, \text{Br}, \text{I}$ ) have been synthesized,<sup>22–</sup>

<sup>24</sup> but reports of their properties are sparse. CsEuCl<sub>3</sub> and CsEuBr<sub>3</sub> have published crystal structures, but only the lattice constants of CsEuI<sub>3</sub> have been reported. The temperature-dependent magnetic susceptibility of CsEuBr<sub>3</sub> was measured above 5 K with no observed magnetic transitions, though its Weiss temperature of -2.4 K suggests that antiferromagnetic interactions are present.<sup>23</sup> The magnetism of bulk CsEuCl<sub>3</sub> and CsEuI<sub>3</sub> have not been reported. Thin films and nanocrystals of CsEuCl<sub>3</sub> were recently reported to be ferromagnetic with Curie temperatures of 2.5-3.0 K,<sup>25</sup> but the magnetism of nanocrystalline and thin film samples can differ from bulk samples due to substrate-induced strain or surface reconstruction and large surface-to-volume ratios resulting in multiple metal oxidation states.<sup>26,27</sup>

We demonstrate that CsEuBr<sub>3</sub> and CsEuCl<sub>3</sub> are magnetic semiconductors that order antiferromagnetically at Néel temperatures  $T_N$  of 2.0 K and 1.0 K respectively. Heat capacity measurements confirm the presence of a bulk phase transition at these temperatures.<sup>28</sup> Surprisingly, the magnitude of the heat capacity anomalies indicate that while CsEuBr<sub>3</sub> exhibits conventional equal-moment antiferromagnetism, CsEuCl<sub>3</sub> instead exhibits amplitude-modulated antiferromagnetism where the magnetic moment periodically and incommensurately varies within the structure.<sup>28</sup> Antiferromagnetism in these materials is consistent with the Goodenough-Kanamori rule for  $\sim 180^\circ$  magnetic superexchange interactions through an anion with filled valence orbitals,<sup>29</sup> and density-functional theory calculations support the antiferromagnetic superexchange mechanism. This is the first report of antiferromagnetic ordering in a pure-phase halide perovskite with a rare earth element on the B-site, demonstrating that rare earth halide perovskites can be considered for use in spintronic devices. Furthermore, our finding of antiferromagnetism in bulk CsEuCl<sub>3</sub> in contrast to the previous report of ferromagnetism in nanocrystals and thin films<sup>25</sup>

shows that confinement and/or strain can be used to tune magnetic interactions in halide perovskites from antiferromagnetic to ferromagnetic.<sup>26,27</sup>

Figure 1A shows powder X-ray diffraction patterns of CsEuBr<sub>3</sub> (black) and CsEuCl<sub>3</sub> (red) compared with computed patterns from reported crystal structures (blue and orange).<sup>22,23</sup> CsEuBr<sub>3</sub> is orthorhombic at room temperature, with 155.97(7)° and 162.09(10)° interoctahedral Eu-Br-Eu bond angles (Figure 1B), while CsEuCl<sub>3</sub> is a much less distorted tetragonal perovskite (Figure 1C) because of the smaller size of Cl. It has 177.235(5)° and 180° Eu-Cl-Eu bond angles. CsEuBr<sub>3</sub> and CsEuCl<sub>3</sub> have bandgaps of 2.90(4) and 2.91(5) eV (Figure 1D-E), which originate from the Eu<sup>2+</sup> *f-d* electronic transition.<sup>30</sup>

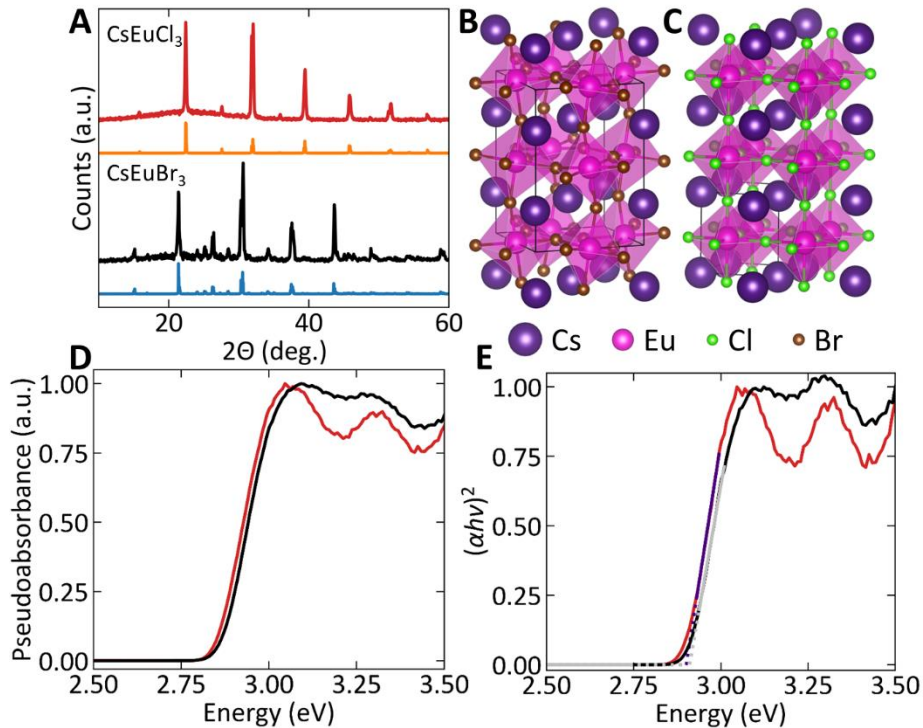


**Figure 1: Characterization.** A) Powder diffraction patterns of CsEuBr<sub>3</sub> (black) and CsEuCl<sub>3</sub> (red) with simulated patterns (blue, orange) from reported crystal structures.<sup>22,23</sup> Depiction of structures of B) CsEuBr<sub>3</sub> and C) CsEuCl<sub>3</sub>. D) Pseudoabsorbance spectra of CsEuBr<sub>3</sub> (black) and CsEuCl<sub>3</sub> (red). E) Direct bandgap Tauc plots for CsEuBr<sub>3</sub> (black, with bandgap fit in grey) and CsEuCl<sub>3</sub> (red, with bandgap fit in purple).

Figure 2A shows the zero-field-cooled magnetic susceptibility ( $\chi$ ) of CsEuBr<sub>3</sub> using a 1000 Oe field-(black) with a fit (white) to the Curie-Weiss law

$$\chi = \frac{C}{T - \Theta} + \chi_0 \quad 1$$

as well as the inverse susceptibility  $(\chi - \chi_0)^{-1}$  (blue), which is linear. The Curie constant  $C = 8.534(6)$  emu·K/mol, resulting in a computed magnetic moment per Eu<sup>2+</sup> of 8.26  $\mu_B$ , which is only 4% larger than the spin-only moment for Eu<sup>2+</sup> ( $J = 7/2$ ) of 7.94  $\mu_B$ . The Weiss temperature  $\Theta = -4.57(2)$  K, and a negative Weiss temperature indicates the dominance of antiferromagnetic coupling in the material. It is similar to a previously reported value of -2.4 K.<sup>23</sup>  $\chi_0 = -2.50(2) \times 10^{-3}$  emu/mol.

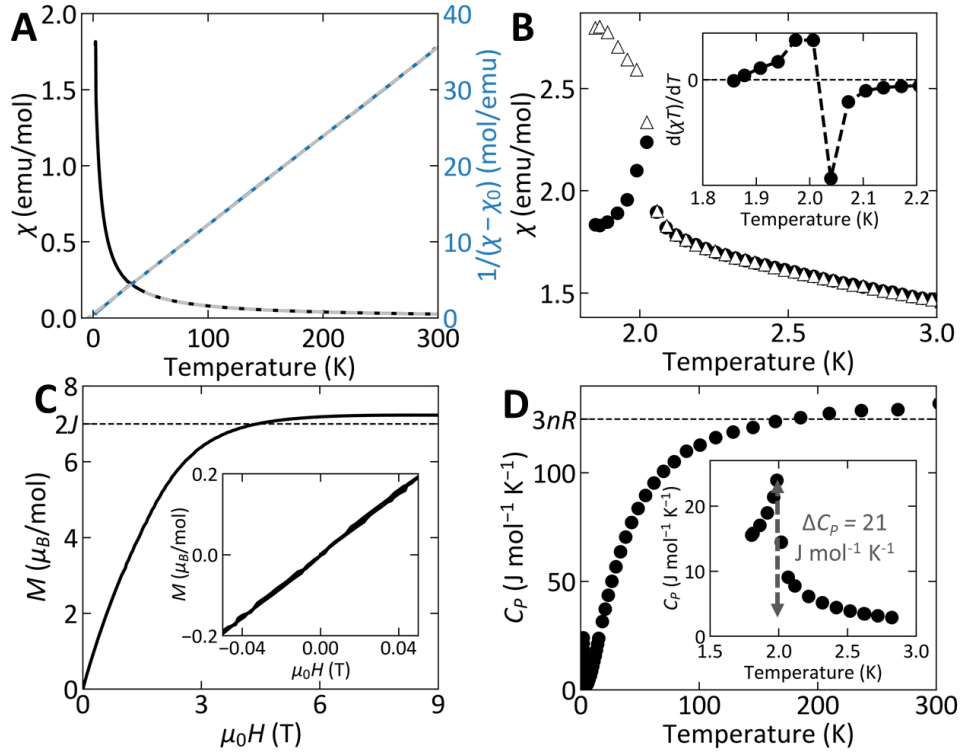


**Figure 2: CsEuBr<sub>3</sub> magnetism.** A) Field-dependent susceptibility at 1000 Oe (black) with Curie-Weiss fit (white) and inverse susceptibility (blue) with linear fit (grey). B) Zero-field- (circles) and field-cooled (triangles) susceptibility at 10 Oe. Inset: first derivative of zero-field-cooled  $\chi T$ . C) Field-dependent magnetization at 1.9 K. D) Constant-pressure heat capacity.

The zero-field-cooled (circles) and field-cooled (triangles) magnetic susceptibilities at a field of 10 Oe are plotted in Figure 2B. There is a discontinuity in the zero field-cooled susceptibility (inset, Figure 2B) at 2.0 K, and the downturn in  $\chi$  combined with its low value suggests the onset of antiferromagnetic ordering at a Neél temperature  $T_N = 2.0$  K. The onset of antiferromagnetic ordering was not observed previously because the susceptibility was only measured above 5 K.<sup>23</sup> There is no hysteresis in the field-dependent magnetization collected at 1.9 K (Figure 2C), further suggesting the presence of antiferromagnetic ordering. The field-dependent magnetization at 1.9 K saturates at  $\mu_0 H = 6$  T because the weak antiferromagnetic interactions between spins are overcome by the applied field.

The second-order anomaly at 2.0 K in the heat capacity of CsEuBr<sub>3</sub> (Figure 2D) confirms the presence of a bulk phase transition, and the 21 J/K·mol magnitude is in line with the theoretical value of 20.14 J/K·mol for the heat capacity anomaly upon the transition to equal-moment antiferromagnetism state, where the magnitude of the moment is the same on every Eu<sup>2+</sup> ion.<sup>28,31</sup>

The red line in Figure 3A shows the zero-field-cooled magnetization of CsEuCl<sub>3</sub> at a field of 100 Oe with a fit to the Curie-Weiss law in white.  $\theta = -3.06(1)$  K, indicating antiferromagnetic coupling dominates like in CsEuBr<sub>3</sub>.  $C = 7.123(9)$  emu·K/mol, which corresponds to a moment per Eu<sup>2+</sup> of 7.55  $\mu_B$ , deviating by 5% from the ideal spin-only moment of Eu<sup>2+</sup> (7.94  $\mu_B$ ).  $\chi_0 = -1.61(2) \times 10^{-3}$  emu/mol. No magnetic phase transition is apparent between 1.8 and 300 K.

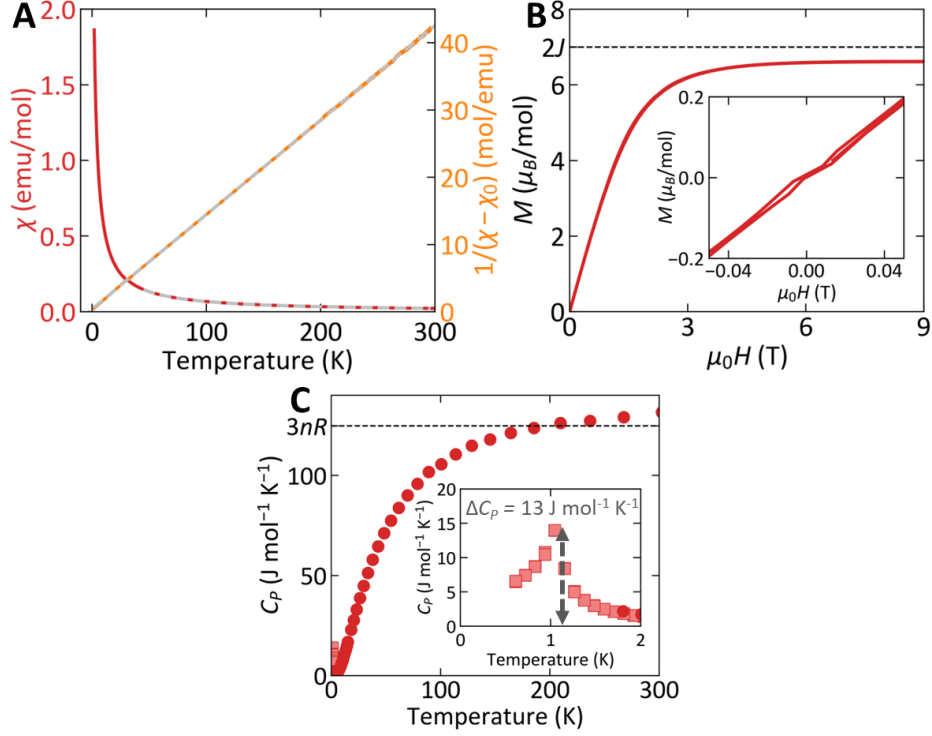


**Figure 3: CsEuCl<sub>3</sub> magnetism.** A) Field-dependent susceptibility at 100 Oe (red) with Curie-Weiss fit (grey) and inverse susceptibility (orange) with linear fit (grey). B) Field-dependent magnetization at 1.8 K. C) Constant-pressure heat capacity.

To further investigate the magnetic properties of CsEuCl<sub>3</sub>, we measured its heat capacity from 0.6 to 300 K. We find a discontinuity at 1.0 K where the heat capacity increases by 13 J/K·mol. This change is consistent with a phase transition to an amplitude-modulated antiferromagnetic state, where the theoretical jump in heat capacity is 13.4 J/K·mol, 2/3 of what is found in the transition to an equal-moment antiferromagnetic order like in CsEuBr<sub>3</sub>.<sup>28,31</sup> In an amplitude-modulated antiferromagnet, there is a periodic variation of the magnetic moment on each magnetic ion which is incommensurate with the lattice, and the smaller jump in specific heat is caused by the periodicity because not all spins are ordered on every ion.

The Goodenough-Kanamori rules can be used to predict and rationalize the magnetism of extended solids through superexchange interactions, which occur when a closed-shell ion (here,

Cl<sup>-</sup> or Br<sup>-</sup>) bridges two open-shell ions (here, Eu<sup>2+</sup>).<sup>29</sup> When the two open-shell ions have the same number of unpaired electrons and the angle formed by the three atoms is close to 180°, antiferromagnetism is expected because the exchange interaction occurs through the same orbital of the closed-shell ion, and the Pauli exclusion principle requires the spins on the ions to be antiparallel to one another. If the angle is instead 90°, the exchange interaction can occur through two orthogonal *p* orbitals where the Pauli exclusion principle does not apply, so the spins will likely interact ferromagnetically.

The magnetism of both CsEuBr<sub>3</sub> and CsEuCl<sub>3</sub> can be rationalized through the Goodenough-Kanamori rules. They are both perovskites, so the Eu-X-Eu angle is close to 180° (Figure 1B-C). Both CsEuBr<sub>3</sub> and CsEuCl<sub>3</sub> should thus be antiferromagnetic, matching our experimental observations. Antiferromagnetism is consistent with what is observed in other magnetic halide perovskites such as KMF<sub>3</sub> (M = Mn, Fe, Co, Ni, Cu) and KMnCl<sub>3</sub>, which all order antiferromagnetically with Néel temperatures ranging from 88-275 K.<sup>16,18</sup>

We next use density-functional theory calculations<sup>32-34</sup> to visualize the magnetic interactions in CsEuBr<sub>3</sub> and CsEuCl<sub>3</sub> and confirm the applicability of the Goodenough-Kanamori rules in rare earth-containing magnetic halide perovskites. Figure 4 depicts the computed spin polarization for CsEuBr<sub>3</sub> and CsEuCl<sub>3</sub> in the (101) plane, where the spin polarization is defined as the difference between the spin-up (red) and spin-down (blue) electron density—if the spin-up and spin-down electron densities are equal, the spin polarization is zero. Eu<sup>2+</sup> has seven unpaired *f* electrons in its ground state. If the valence electrons on a given Eu<sup>2+</sup> are spin-up (red, Figure 4), then the halide *p*-electrons bonding with this Eu<sup>2+</sup> must be spin-down (blue, Figure 4) because of the Pauli exclusion rule. The other electron in this orbital must be spin-up, so the other Eu<sup>2+</sup> bonded to this halogen must be spin-down, resulting in antiferromagnetism.

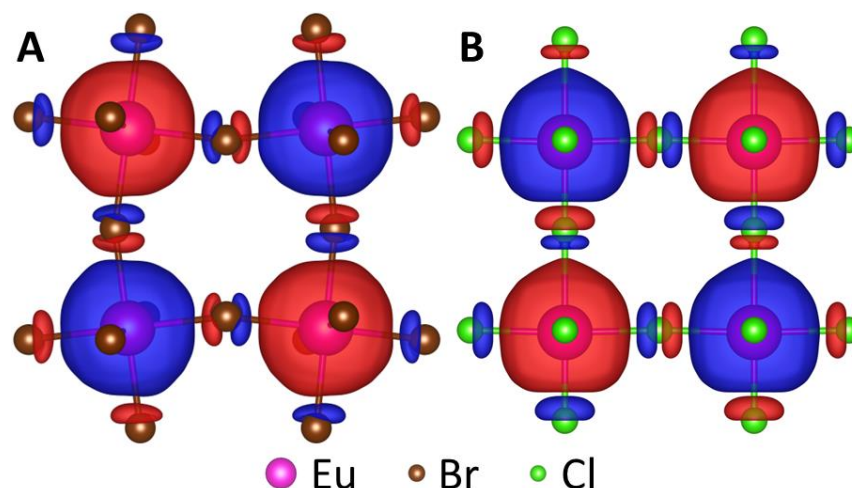


**Figure 4: Magnetic superexchange.** The spin-polarized charge density of (A) CsEuBr<sub>3</sub> and (B) CsEuCl<sub>3</sub> in the <101> plane at 0.0003 e/a<sub>0</sub><sup>3</sup> with spin-up density in red and spin-down density in blue.

The Néel temperatures of CsEuBr<sub>3</sub> and CsEuCl<sub>3</sub> are similar to the temperature at which other Eu<sup>2+</sup>-containing halides magnetically order. EuF<sub>2</sub> orders antiferromagnetically at 1.0 K,<sup>35</sup> EuCl<sub>2</sub> and EuI<sub>2</sub> ferromagnetically at 1.64 and 1.75 K, and EuBr<sub>2</sub> is paramagnetic with no magnetic ordering above 1.1 K.<sup>36</sup> EuF<sub>2</sub> is cubic and adopts the CaF<sub>2</sub> structure type, with Eu-F-Eu bond angles of 109.5°.<sup>37</sup> EuCl<sub>2</sub>, EuBr<sub>2</sub>, and EuI<sub>2</sub> are more complicated structures with multiple Eu-X-Eu bond angles in each structure that range from 82-118°;<sup>36</sup> their ferromagnetism is expected from Goodenough-Kanamori rules because of the near 90° bond angles.<sup>29</sup> The layered organic-inorganic hybrid perovskite (C<sub>4</sub>H<sub>9</sub>NH<sub>3</sub>)<sub>2</sub>EuI<sub>4</sub> does not order above 1.8 K and has a Weiss temperature of -2 K, consistent with its Eu-I-Eu bond angles near 180°.<sup>38</sup>

A previous report determined that nanocrystals and thermally evaporated thin films of CsEuCl<sub>3</sub> are ferromagnetic with Curie temperatures of 2.5-3.0 K using magnetic circular dichroism measurements.<sup>25</sup> Nanocrystalline and thin film samples may behave differently than bulk materials because of differences in preparation, interactions with the substrate, or the formation of Eu<sup>3+</sup> in addition to Eu<sup>2+</sup> to compensate for the presence of excess Cl<sup>-</sup> or deficiency of Cs<sup>+</sup>. The oxide perovskite LaMnO<sub>3</sub>, for example, is antiferromagnetic when prepared as a bulk material, but thin

films of  $\text{LaMnO}_3$  can be ferromagnetic.<sup>26,27</sup> The onset of ferromagnetism has been rationalized as either the result of strain in the thin film<sup>27</sup> or the formation of  $\text{Mn}^{4+}$  to compensate for excess oxygen content.<sup>26</sup> We believe that ferromagnetism is unlikely in *bulk*  $\text{CsEuCl}_3$  because of its negative  $\Theta$ , the presence of the heat capacity anomaly at 1.0 K with a magnitude consistent with the transition to an amplitude-modulated antiferromagnetic state, and the prediction of antiferromagnetism from the Goodenough-Kanamori rules. The transition from antiferromagnetism in bulk  $\text{CsEuCl}_3$  to ferromagnetism in thin film and nanocrystalline  $\text{CsEuCl}_3$  demonstrates that it may be possible to tune the magnetic interactions in magnetic halide perovskites through substrate or surface effects, allowing for the creation of spintronic circuits with both ferromagnetic and antiferromagnetic components using a single material such as  $\text{CsEuCl}_3$  as the only magnetic material.

We discover that the semiconducting halide perovskites  $\text{CsEuBr}_3$  and  $\text{CsEuCl}_3$  order antiferromagnetically at 2.0 K and 1.0 K. The magnitudes of the heat capacity anomalies suggest that the magnitude of the moments on each  $\text{Eu}^{2+}$  are equal in  $\text{CsEuBr}_3$  but vary periodically and incommensurately in  $\text{CsEuCl}_3$ ; neutron diffraction measurements will be needed to confirm their magnetic structure.  $\text{CsEuBr}_3$  and  $\text{CsEuCl}_3$  are the first examples of bulk rare-earth halide perovskites that exhibit magnetic order. Furthermore, the type and degree of magnetic coupling in  $\text{CsEuCl}_3$  can likely be tuned from antiferromagnetic to ferromagnetic through quantum confinement or substrate-film interactions because nanocrystals and thin films of  $\text{CsEuCl}_3$  were previously reported to be ferromagnetic.<sup>25</sup> The observation of magnetic ordering in bulk  $\text{CsEuBr}_3$  and  $\text{CsEuCl}_3$  expands the possible applications of chloride, bromide, and iodide halide perovskites beyond optical and electronic devices to now include spintronic devices.

## Methods

CsEuBr<sub>3</sub> was synthesized by placing a stoichiometric amount of CsBr (Sigma-Aldrich, 99.999%, anhydrous) and EuBr<sub>2</sub> (Alfa Aesar, 99.99%) in a quartz tube inside an argon-filled glove box. The tube was then evacuated and flushed with argon three times before being ampouled under vacuum ( $10^{-3}$  torr). The ampoule was heated in a furnace to 900 °C for 12 hours before being cooled to room temperature at a rate of 6 °C/hour and was subsequently opened in a nitrogen-filled glove box. CsEuCl<sub>3</sub> was synthesized similarly to CsEuBr<sub>3</sub> using CsCl (Alfa Aesar, 99.9%, ultra-dry) and EuCl<sub>2</sub> (Sigma-Aldrich, 99.99%).

X-ray diffraction measurements were performed on a Rigaku Miniflex II diffractometer using Cu  $\alpha$  radiation located inside a nitrogen-filled glove box. Diffuse reflectance spectra were collected using an Agilent Cary 5000 equipped with a DRA-2500 internal integrating sphere accessory on material diluted to approximately 15% w/w with dry MgO powder (Alfa Aesar, 99.95%) using Agilent powder sample holders sealed with an O-ring. Magnetic susceptibility and heat capacity data were collected with a Quantum Design EverCool II or a Dynacool PPMS. Magnetization was measured with a vibrating sample magnetometer (VSM) on powders or polycrystalline pieces of material in plastic holders. No diamagnetic corrections were applied for the material or sample holder. Heat capacity measurements used the two-tau relaxation method on polycrystalline pieces of material. Heat capacity measurements below 1.8 K on CsEuCl<sub>3</sub> used a <sup>3</sup>He refrigerator.

Density-functional theory calculations were performed using Quantum Espresso version 7.0<sup>32,33</sup> using the spin-polarized generalized gradient approximation with and PBE exchange-correlation functional.<sup>39,40</sup> SCF calculations used the GPU-enabled version of Quantum Espresso.<sup>34</sup> Scalar-relativistic pseudopotentials from the Standard Solid State Pseudopotentials

precision collection v1.12 were used.<sup>41–44</sup> The structures of CsEuCl<sub>3</sub> and CsEuBr<sub>3</sub> were downloaded from the Inorganic Crystal Structure Database<sup>45</sup> and were originally reported in references 22,23. For CsEuCl<sub>3</sub>, the tetragonal cell was converted to a  $\sqrt{2} \times \sqrt{2} \times 2$  supercell to allow antiferromagnetism to be modeled. Spin polarization is restricted to the *z* direction, and the total magnetization is set to 0.

## Acknowledgments

This work is supported by the Gordon and Betty Moore Foundation as part of the EPiQS initiative under grant GBMF9066. The work at Gdańsk Tech. was supported by the National Science Centre (Poland; Grant UMO-2018/30/M/ST5/00773). Density-functional theory calculations used computational resources managed and supported by Princeton Research Computing, a consortium of groups including the Princeton Institute for Computational Science and Engineering (PICSciE) and the Office of Information Technology's High Performance Computing Center and Visualization Laboratory at Princeton University

## References

- (1) Saporov, B.; Mitzi, D. B. Organic–Inorganic Perovskites: Structural Versatility for Functional Materials Design. *Chem. Rev.* **2016**, *116*, 4558–4596.
- (2) Mitchell, R. H. *Perovskites: Modern and Ancient*; Almaz Press: Thunder Bay, 2002.
- (3) Filip, M. R.; Giustino, F. The Geometric Blueprint of Perovskites. *Proc. Natl. Acad. Sci.* **2018**, *115*, 5397–5402.
- (4) Goldschmidt, V. M. Crystal Structure and Chemical Constitution. *Trans. Faraday Soc.* **1929**, *25*, 253.
- (5) Mitzi, D. B. Synthesis, Structure, and Properties of Organic-Inorganic Perovskites and Related Materials. *Prog. Inorg. Chem.* **1999**, *48*, 1–121.
- (6) Dong, Q.; Fang, Y.; Shao, Y.; Mulligan, P.; Qiu, J.; Cao, L.; Huang, J. Electron-Hole Diffusion Lengths > 175 $\mu$ m in Solution-Grown CH<sub>3</sub>NH<sub>3</sub>PbI<sub>3</sub> Single Crystals. *Science* **2015**, *347*, 967–970.

- (7) NREL. Best Research-Cell Efficiencies <http://www.nrel.gov/pv/assets/images/efficiency-chart.png> (accessed Jan 27, 2022).
- (8) Jena, A. K.; Kulkarni, A.; Miyasaka, T. Halide Perovskite Photovoltaics: Background, Status, and Future Prospects. *Chem. Rev.* **2019**, *119*, 3036–3103.
- (9) Chuang, P.; Ho, S. C.; Smith, L. W.; Sfigakis, F.; Pepper, M.; Chen, C. H.; Fan, J. C.; Griffiths, J. P.; Farrer, I.; Beere, H. E.; Jones, G. A. C.; Ritchie, D. A.; Chen, T. M. All-Electric All-Semiconductor Spin Field-Effect Transistors. *Nat. Nanotechnol.* **2015**, *10*, 35–39.
- (10) Dietl, T. A Ten-Year Perspective on Dilute Magnetic Semiconductors and Oxides. *Nat. Mater.* **2010**, *9*, 965–974.
- (11) Awschalom, D. D.; Flatté, M. E. Challenges for Semiconductor Spintronics. *Nat. Phys.* **2007**, *3*, 153–159.
- (12) Cava, R.; de Leon, N.; Xie, W. Introduction: Quantum Materials. *Chem. Rev.* **2021**, *121*, 2777–2779.
- (13) Nguyen, L. T.; Cava, R. J. Hexagonal Perovskites as Quantum Materials. *Chem. Rev.* **2021**, *121*, 2935–2965.
- (14) Chamorro, J. R.; McQueen, T. M.; Tran, T. T. Chemistry of Quantum Spin Liquids. *Chem. Rev.* **2021**, *121*, 2898–2934.
- (15) Kagan, C. R.; Bassett, L. C.; Murray, C. B.; Thompson, S. M. Colloidal Quantum Dots as Platforms for Quantum Information Science. *Chem. Rev.* **2021**, *121*, 3186–3233.
- (16) Okazaki, A.; Suemune, Y. The Crystal Structures of  $\text{KMnF}_3$ ,  $\text{KFeF}_3$ ,  $\text{KCoF}_3$ ,  $\text{KNiF}_3$  and  $\text{KCuF}_3$  above and below Their Néel Temperatures. *J. Phys. Soc. Japan* **1961**, *16*, 671–675.
- (17) De Jongh, L. J.; Miedema, A. R. Experiments on Simple Magnetic Model Systems. *Adv. Phys.* **2001**, *50*, 947–1170.
- (18) Harris, P.; Larsen, S.; Lebech, B. A Single Crystal Neutron Diffraction Study of  $\text{KMnCl}_3$ . Its Twinning and Magnetic Structure. *J. Phys. Chem. Solids* **1992**, *53*, 1021–1025.
- (19) Horowitz, A.; Amit, M.; Makovsky, J.; Dor, L. Ben; Kalman, Z. H. Structure Types and Phase Transformations in  $\text{KMnCl}_3$  and  $\text{TlMnCl}_3$ . *J. Solid State Chem.* **1982**, *43*, 107–125.
- (20) Straus, D. B.; Guo, S.; Cava, R. J. Kinetically Stable Single Crystals of Perovskite-Phase  $\text{CsPbI}_3$ . *J. Am. Chem. Soc.* **2019**, *141*, 11435–11439.
- (21) Straus, D. B.; Kagan, C. R. Photophysics of Two-Dimensional Semiconducting Organic–Inorganic Metal-Halide Perovskites. *Annu. Rev. Phys. Chem.* **2022**, *73*, 403–428.
- (22) Nocera, D. G.; Morss, L. R.; Fahey, J. A. Preparation, Crystal Structure, and Enthalpy of Formation of Cesium Europium(II) Chloride,  $\text{CsEuCl}_3$ . *J. Inorg. Nucl. Chem.* **1980**, *42*, 55–59.
- (23) Ehrenberg, H.; Fuess, H.; Hesse, S.; Zimmermann, J.; von Seggern, H.; Knapp, M.

- Structures of CsEuBr<sub>3</sub> and Its Degradation Product Cs<sub>2</sub>EuBr<sub>5</sub> · 10H<sub>2</sub>O. *Acta Crystallogr. Sect. B Struct. Sci.* **2007**, *63*, 201–204.
- (24) Baopeng, C.; Shihua, W.; Xinhua, Z. Synthesis and Structure of AEuI<sub>3</sub> (ARb, Cs) and AEu<sub>2</sub>I<sub>5</sub> (AK, Rb, Cs). *J. Alloys Compd.* **1992**, *181*, 511–514.
- (25) Walsh, K. M.; Pressler, K.; Crane, M. J.; Gamelin, D. R. Ferromagnetism and Spin-Polarized Luminescence in Lead-Free CsEuCl<sub>3</sub> Perovskite Nanocrystals and Thin Films. *ACS Nano* **2022**, *16*, 2569–2576.
- (26) Niu, W.; Liu, W.; Gu, M.; Chen, Y.; Zhang, X.; Zhang, M.; Chen, Y.; Wang, J.; Du, J.; Song, F.; Pan, X.; Pryds, N.; Wang, X.; Wang, P.; Xu, Y.; Chen, Y.; Zhang, R. Direct Demonstration of the Emergent Magnetism Resulting from the Multivalence Mn in a LaMnO<sub>3</sub> Epitaxial Thin Film System. *Adv. Electron. Mater.* **2018**, *4*, 1–9.
- (27) Roqueta, J.; Pomar, A.; Balcells, L.; Frontera, C.; Valencia, S.; Abrudan, R.; Bozzo, B.; Konstantinović, Z.; Santiso, J.; Martínez, B. Strain-Engineered Ferromagnetism in LaMnO<sub>3</sub> Thin Films. *Cryst. Growth Des.* **2015**, *15*, 5332–5337.
- (28) Blanco, J. A.; Gignoux, D.; Schmitt, D. Specific Heat in Some Gadolinium Compounds. II. Theoretical Model. *Phys. Rev. B* **1991**, *43*, 13145–13151.
- (29) Goodenough, J. B. *Magnetism and the Chemical Bond*; Interscience Publishers: New York, 1963.
- (30) Tsu, R.; Esaki, L. Luminescence Spectra of Europium Chalcogenides: EuO, EuS, and EuSe. *Phys. Rev. Lett.* **1970**, *24*, 455–459.
- (31) Bednarchuk, O.; Gagor, A.; Kaczorowski, D. Synthesis, Crystal Structure and Physical Properties of EuTGe<sub>3</sub> (T = Co, Ni, Rh, Pd, Ir, Pt) Single Crystals. *J. Alloys Compd.* **2015**, *622*, 432–439.
- (32) Giannozzi, P.; Baroni, S.; Bonini, N.; Calandra, M.; Car, R.; Cavazzoni, C.; Ceresoli, D.; Chiarotti, G. L.; Cococcioni, M.; Dabo, I.; Dal Corso, A.; de Gironcoli, S.; Fabris, S.; Fratesi, G.; Gebauer, R.; Gerstmann, U.; Gougoussis, C.; Kokalj, A.; Lazzeri, M.; et al. QUANTUM ESPRESSO: A Modular and Open-Source Software Project for Quantum Simulations of Materials. *J. Phys. Condens. Matter* **2009**, *21*, 395502.
- (33) Giannozzi, P.; Andreussi, O.; Brumme, T.; Bunau, O.; Nardelli, M. B.; Calandra, M.; Car, R.; Cavazzoni, C.; Ceresoli, D.; Cococcioni, M.; others. Advanced Capabilities for Materials Modelling with Quantum ESPRESSO. *J. Phys. Condens. Matter* **2017**, *29*, 465901.
- (34) Giannozzi, P.; Baseggio, O.; Bonfà, P.; Brunato, D.; Car, R.; Carnimeo, I.; Cavazzoni, C.; De Gironcoli, S.; Delugas, P.; Ferrari Ruffino, F.; Ferretti, A.; Marzari, N.; Timrov, I.; Urru, A.; Baroni, S. Quantum ESPRESSO toward the Exascale. *J. Chem. Phys.* **2020**, *152*.
- (35) Ehnholm, G. J.; Katila, T. E.; Lounasmaa, O. V.; Reivari, P.; Kalvius, G. M.; Shenoy, G. K. Mössbauer Study of Hyperfine Interactions in Divalent Europium Compounds at Ultra Low Temperatures. *Zeitschrift für Phys.* **1970**, *235*, 289–307.
- (36) Sanchez, J. P.; Friedt, J. M.; Bärnighausen, H.; Van Duyneveldt, A. J. Structural,

- Magnetic, and Electronic Properties of Europium Dihalides,  $\text{EuX}_2$  ( $X = \text{Cl}, \text{Br}, \text{I}$ ). *Inorg. Chem.* **1985**, *24*, 408–415.
- (37) Beck, G.; Nowacki, W. Herstellung Und Kristallstruktur von  $\text{EuS}$  Und  $\text{EuF}_2$ . *Naturwissenschaften* **1938**, *26*, 495–496.
- (38) Mitzi, D. B.; Liang, K. Preparation and Properties of  $(\text{C}_4\text{H}_9\text{NH}_3)_2\text{EuI}_4$ : A Luminescent Organic-Inorganic Perovskite with a Divalent Rare-Earth Metal Halide Framework. *Chem. Mater.* **1997**, *9*, 2990–2995.
- (39) Perdew, J. P.; Burke, K.; Ernzerhof, M. Generalized Gradient Approximation Made Simple. *Phys. Rev. Lett.* **1996**, *77*, 3865–3868.
- (40) Dal Corso, A.; de Gironcoli, S. Ab Initio Phonon Dispersions of Fe and Ni. *Phys. Rev. B* **2000**, *62*, 273–277.
- (41) Prandini, G.; Marrazzo, A.; Castelli, I. E.; Mounet, N.; Marzari, N. Precision and Efficiency in Solid-State Pseudopotential Calculations. *npj Comput. Mater.* **2018**, *4*.
- (42) Dal Corso, A. Pseudopotentials Periodic Table: From H to Pu. *Comput. Mater. Sci.* **2014**, *95*, 337–350.
- (43) Garrity, K. F.; Bennett, J. W.; Rabe, K. M.; Vanderbilt, D. Pseudopotentials for High-Throughput DFT Calculations. *Comput. Mater. Sci.* **2014**, *81*, 446–452.
- (44) Topsakal, M.; Wentzcovitch, R. M. Accurate Projected Augmented Wave (PAW) Datasets for Rare-Earth Elements ( $\text{RE} = \text{La-Lu}$ ). *Comput. Mater. Sci.* **2014**, *95*, 263–270.
- (45) Hellenbrandt, M. The Inorganic Crystal Structure Database (ICSD) - Present and Future. In *Crystallography Reviews*; 2004; Vol. 10, pp 17–22.